Density fluctuations in liquid neon studied by neutron scattering

A. A. van Well and L. A. de Graaf
Interuniversitair Reactor Instituut, NL-2629JB Delft, The Netherlands
(Received 22 April 1985)

Inelastic neutron scattering experiments have been performed on liquid neon at a temperature of 35 K and pressures of 8 and 14 MPa. The spectra were corrected for all known experimental effects. Normalized results for the coherent dynamic structure factor $S(k,\omega)$ were obtained for wave numbers k between 3 and 22 nm^{-1}, all below the position of the first peak, at $k_0=23.5$ nm^{-1}, in the static structure factor $S(k)$. The $S(k)$, calculated by numerical integration of $S(k,\omega)$, is compared with neutron diffraction data and with $S(k)$ of argon at corresponding thermodynamic conditions. Quantum corrections to the second frequency moment of $S(k,\omega)$ are examined, and a quasiclassical approximation of $S(k,\omega)$ is discussed. When comparing $S(k,\omega)$ of neon and argon it appears that, except for some small deviations, the principle of corresponding states is valid. The experimental data can well be described by means of one (extended) heat mode and two (extended) sound modes. The sound modes are clearly manifest as shoulders in $S(k,\omega)$ which shift, for increasing k, to larger ω and disappear gradually as k approaches k_0. The obtained sound dispersion curve, including a sound propagation gap near k_0, is consistent with theoretical predictions and with recent results from neutron scattering experiments on argon and from computer simulations. An interpretation in terms of k-dependent transport coefficients is discussed.

I. INTRODUCTION

Inelastic neutron scattering (INS) is a powerful technique to study density fluctuations in liquids on an atomic scale. The dynamic structure factor $S(k,\omega)$, which is directly connected to the neutron scattering cross section, reflects density fluctuations with wavelength $\lambda=2\pi/k$ and frequency ω. Recently, $S(k,\omega)$ data with high statistical accuracy have been obtained for liquid ^{36}Ar at 120 K and various pressures between 2 and 85 MPa from neutron scattering at the reactors of the Interuniversitair Reactor Instituut (IRI) in Delft[1] and of the Institut Laue-Langevin in Grenoble.[2] Most of these experiments covered the wave-number range $4\lesssim k\lesssim 40$ nm^{-1}, representing fluctuations with wavelengths $0.5\sigma\lesssim\lambda\lesssim 4.5\sigma$, σ being the diameter of the atoms. Although the obtained $S(k,\omega)$ is a seemingly featureless function of ω in this k range, it was found that it can well be described in terms of three extended hydrodynamic modes[3]

$$S(k,\omega)=S(k)\mathrm{Re}\left[\sum_{j=-1}^{+1}\frac{1}{\pi}\frac{A_j(k)}{i\omega+z_j(k)}\right], \quad (1)$$

where $A_0(k)$ and $z_0(k)$ are real, $A_{\pm1}(k)$ and $z_{\pm1}(k)$ are either real or complex conjugate pairs, and $S(k)$ is the static structure factor. For small k Eq. (1) goes over continuously into the Landau-Placzek triplet of one Rayleigh (heat, $j=0$) and two Brillouin (sound, $j=\pm1$) lines. For argon $S(k,\omega)$ is dominated by the extended heat mode which is always centered around $\omega=0$, while the shape is co-determined by two heavily damped extended sound modes. The sound modes are centered around $\omega\neq0$, except for k values near the main peak in $S(k)$, where for most conditions a gap in the sound dispersion curve occurs. The width of the dispersion gap decreases with increasing pressure and the gap has vanished at 85 MPa. These observations were confirmed by results from computer molecular dynamics (CMD) simulations of systems with Lennard-Jones (LJ) and purely repulsive interparticle potentials.[4]

The possibility to describe $S(k,\omega)$ in terms of three extended hydrodynamic modes has been predicted using a generalized Enskog kinetic theory for hard-sphere fluids.[5] The main features of $S(k,\omega)$ calculated from this theory, i.e., the k dependence of its width[6] and the existence of a sound propagation gap,[7] agree with those found in the experiments.

In this paper we report INS results for neon at two densities at 35 K, which are thermodynamic conditions corresponding with those of the argon measurements mentioned. The measurements were restricted to k values smaller than the position of the main peak of $S(k)$. The motivation for this experiment was threefold.

(i) For studying $S(k,\omega)$ in fluids at small k, neon is more suitable than argon because of the lower adiabatic sound velocity c_s in neon at corresponding thermodynamic conditions. This was already recognized by Bell *et al.*[8] who performed INS measurements on neon at $T=55$ K and a density $n=22.4$ nm^{-3}, and at $T=70$ K, $n=10.1$ and 14.3 nm^{-3} in the range $0.6\lesssim k\lesssim 1.5$ nm^{-1}, where they showed the hydrodynamic description to be valid. They observed deviations from this description at $T=26.5$ K, $n=35.8$ nm^{-3} in the range $2.7<k<15$ nm^{-1}.

For neon at 35 K c_s is about 550 ms^{-1} (compared to 750 ms^{-1} for argon at 120 K) and the kinematic region covered by 5-meV neutrons, having a velocity of 1000 m s^{-1}, will therefore amply include the hydrodynamic dispersion curve $\omega_s=\mathrm{Im}z_{+1}=c_sk$. Moreover, at the same

absolute value of k the physically more-significant reduced quantity $k^*=k\sigma$ is smaller for neon than for argon. These features are clarified in Fig. 1. Here the small-k parts of the kinematic regions of the experiments on argon of Refs. 1 and 2 are compared with that of the present experiment. Wave number k and frequency ω were made dimensionless by the LJ parameters σ and ε and the particle mass M given in Table I.

(ii) The corresponding state principle (CSP) of thermodynamic and transport properties of inert gases has been the subject of many investigations. Using neutron scattering data the CSP can be studied at a microscopic scale. By comparing $S(k)$ of argon from Refs. 1 and 2 with $S(k)$ of neon from neutron diffraction (ND) data[10] deviations of up to 20% are found around $k^*=2$. Inelastic neutron scattering data on both argon and neon provide the opportunity to confirm these deviations in $S(k)$ and to investigate CSP concerning the dynamic properties.

(iii) Because of the lower temperature and the smaller mass, quantum effects in neon will be more important than in the case of argon. $S(k,\omega)$ in Eq. (1) is derived from theory for a classical system and is symmetric in ω whereas $S(k,\omega)$ measured by INS will obey the detailed-balance condition

$$S(k,\omega)=e^{\beta\hbar\omega}S(k,-\omega)\ , \tag{2}$$

where $\hbar\omega$ is the energy transferred from the neutron to the sample, $\beta=(k_BT)^{-1}$. For the interpretation of the argon results in terms of Eq. (1) we have used the quasiclassical approximation[11]

$$\tilde{S}(k,\omega)=\exp\left[-\frac{\beta\hbar\omega}{2}+\frac{\hbar^2k^2\beta}{8M}\right]S(k,\omega)\ , \tag{3}$$

which is correct to order $\hbar$ and is symmetric in ω. Using the neon data, quantum effects in $S(k,\omega)$ and the validity of the approximation in Eq. (3) can be investigated.

In Sec. II the experiment and the data reduction are described. In Sec. III a comparison is made between neon and argon and quantum contributions to $S(k,\omega)$ are discussed. Next, the results are interpreted in terms of collective modes and in terms of generalized hydrodynamics. Section IV contains some concluding remarks.

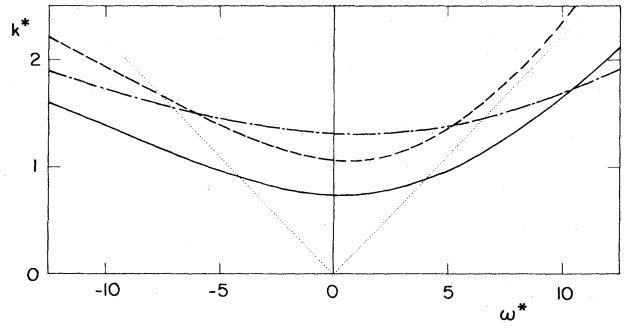

FIG. 1. Kinematic region of TOF spectrometers with the lowest scattering angle indicated: — — —, $\varphi=11.8°$ (Ref. 1); —·—·—·, $\varphi=9.1°$ (Ref. 2); ——, $\varphi=9.9°$ (present experiment). Dispersion curve $\omega^*=c_s^*k^*$ is indicated by dotted line with $c_s^*=c_s\tau/\sigma=4.5$.

TABLE I. Parameters for argon and neon. LJ parameters σ and ε are from Ref. 9. k_B is Boltzmann's constant.

	^{36}Ar	Ne
M (10^{-27} kg)	59.73	33.52
σ (nm)	0.336	0.279
ε/k_B (K)	123.2	36.2
$\tau=\sigma(M/\varepsilon)^{1/2}$ (ps)	1.991	2.285

II. EXPERIMENT AND DATA REDUCTION

A. Measurements

Time-of-flight (TOF) spectra were obtained with the rotating crystal spectrometer RKS 1 at the 2-MW reactor of the IRI in Delft. The incoming neutron wavelength was 0.408 nm (corresponding to an energy of 4.92 meV). ^{3}He detectors of 2.5 cm diameter, placed at 1.20 m from the sample, were combined to 15 detector groups. Relevant data are given in Table II. In each group spectra were recorded in 256 time channels 8 μs wide. The TOF system was triggered twice per revolution of the Pb monochromator crystal defining the period of one duty cycle to be 2209 μs.

We performed five different measurements, of about 200 h each, as indicated in Table III. The vanadium spectra were used for normalization and for determination of the TOF resolution.

The purity of the neon sample was 99.995%. The coherent and incoherent bound-atom cross sections and the absorption cross section for 4.92-meV neutrons are $\sigma_c=2.598(13)$ b, $\sigma_i=0.008(18)$ b, and $\sigma_a=0.088(9)$ b, respectively.[12] The neon container consisted of three high-strength aluminum (Al 7075) tubes, with their center lines 17 mm apart, with 14 mm inner diameter and 1 mm wall thickness, placed in an aluminum frame covered with cadmium (a similar container is described in Ref. 13). The height of the tubes irradiated by the incident neutrons was 53.5 mm. The tubes were placed with their axes perpendicular to the scattering plane; the normal to the plane through the tubes made an angle of +45° with the incident beam. In order to reduce the multiple scattering in the neon sample and the total scattering from the container (which is mainly double Bragg scattering), 0.5-mm-thick boron nitride (BN) disks were inserted in the tubes separated by means of 9.5-mm-high thin-walled aluminum cylinders.

From computer simulations of the experiment with Copley's Monte Carlo program MSCAT (Ref. 14) it appeared that the multiple scattering in neon reduces by a factor of 2 when inserting the BN disks. From the fact that the scattering intensity from the empty neon container equals that from the empty, thinner-walled, vanadium container (see below) we concluded that the BN disks cause a reduction by a factor of 4 in multiple Bragg scattering. The container, surrounded by two radiation shields (one at 35 K and one at liquid-N_2 temperature) was placed in a He flow cryostat. The temperature was measured by a Ge resistor located inside the frame of the container. The absolute accuracy of this thermometer in

TABLE II. Experimental parameters.

Detector group	No. of detectors	Detector length (cm)	Scattering angle (deg)	Angular resolution[a] (deg)	TOF resolution[b] (μs)
1	2	20	9.9	4.8	66
2	2	20	13.8	4.2	68
3	3	20	20.7	3.9	69
4	2	20	27.2	2.7	70
5	2	30	35.2	3.2	73
6	2	30	43.2	3.0	77
7	2	30	51.1	2.9	82
8	2	30	59.1	2.8	85
9	2	30	66.4	2.8	89
10	2	30	75.6	2.8	97
11	1	30	81.9	2.2	100
12	1	30	84.2	2.1	100
13	1	30	89.8	2.0	105
14	1	30	91.0	2.0	105
15	1	30	92.2	2.0	106

[a]FWHM, calculated from dimensions of sample and detectors.
[b]FWHM, determined from elastic part of the vanadium spectrum. TOF from sample to detector for 4.08-Å neutrons was 1236 μs.

the range of interest was 0.01 K. The accuracy of the pressure transducer used was 0.05 MPa. The thermodynamic conditions of the experiment are given in Table III.

The vanadium sample consisted of shavings with lengths of several mm. The geometry of its container was identical to that of the neon container. However, the wall thickness was 0.25 mm and no BN was used. The vanadium filling fraction was 23.4%.

B. Corrections

The experimental data were corrected for constant background, container scattering, multiple scattering, duty-cycle overlap, detector efficiency, TOF resolution and self-shielding, and were normalized absolutely and converted to $S(k,\omega)$ on a rectangular (k,ω) grid.[16] We used the same reduction scheme as was used for the argon measurement in Ref. 2 employing the routines described in Ref. 17. In the following we will discuss a number of correction steps which are of special importance for the present experiment.

The ratio of the intensities scattered by the empty container and by the container filled with neon (vanadium) ranged from 0.9 (0.4) at the smallest to 0.1 (0.2) at the largest scattering angle (see Fig. 2). This implies that the results at the smaller scattering angles will be very sensitive to the correction for container scattering. In this correction f times the (empty) container spectrum was subtracted from the sample spectrum, f representing the time-channel- and angle-dependent attenuation of the container scattering by the sample. Following the method of Copley *et al.*[18] f was calculated for neutrons scattered once in the container. For neon (vanadium) it varied from 0.947 to 0.967 (0.819 to 0.835). Since the coherent cross section of the used aluminum was a factor of 35 larger than the incoherent cross section[13] and since the first Bragg peak occurs at a scattering angle of 120°, the container scattering was mainly double Bragg scattering. This can also be seen in Fig. 2 from the rapid decrease in container scattering with increasing scattering angle, and from the structure due to scattering from container and shields. Thus f will not represent the correct attenuation. From simulations with MSCAT the attenuation of the container scattering by the sample appeared to be equal to f^2 within the statistical uncertainty of 0.02. So, for the

TABLE III. Experimental conditions.

Measurement no.	T (K)	p (MPa)	n (nm^{-3})	Trans.[a]	Scatt.[b]
1 Neon	35.08(1)	8.01(5)	33.36(5)[c]	0.867	0.071
2 Neon	35.08(1)	14.03(5)	34.62(5)[c]	0.862	0.076
3 Ne container	35.08		56.4	0.936	
4 Vanadium	300		16.5[d]	0.711	0.092
5 V container	300		56.4	0.986	

[a]Total transmission (calculated).
[b]Fraction scattered by the sample.
[c]From Ref. 15, n at the critical and triple points are 14.41 and 37.21 nm^{-3}, respectively.
[d]Effective density.

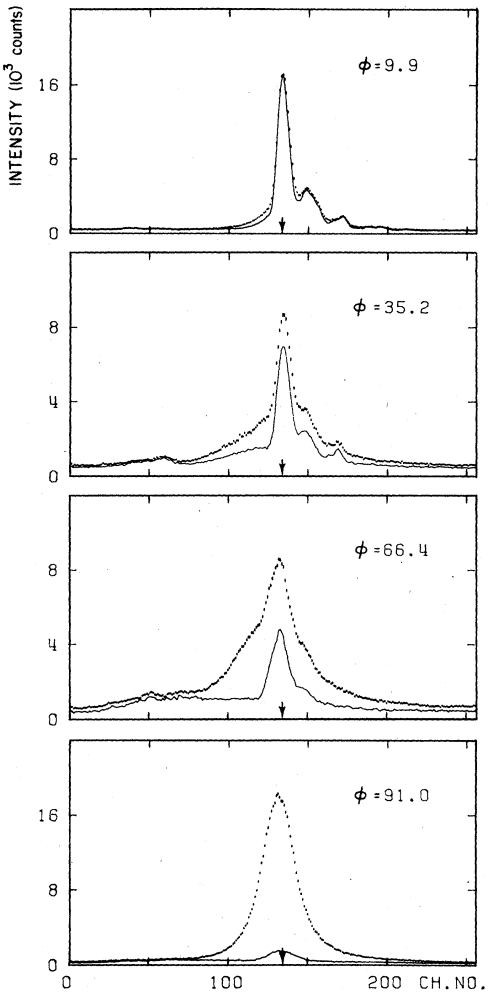

FIG. 2. Raw experimental TOF spectra at four representative scattering angles: error bars, Ne, 35 K, 8 MPa; solid line, empty container; the arrow indicates the position $\omega=0$.

correction we used f^2 (rather than f) and incorporated the uncertainty 0.02 in the calculation of the standard deviations of $S(k,\omega)$. Using f^2 instead of f renders an enhancement of the peak height in the corrected spectra of a factor of 1.7, 1.3, and 1.2 for the three smallest scattering angles, respectively.

It should be noted that the attenuation of the scattering by the aluminum radiation shields and windows of the cryostat is unlikely to be equal to f^2. Although the contribution of this scattering to the total background scattering was small, the fact that we did not use the correct (unknown) attenuation might have led to some systematic error in the corrected spectra at the smaller scattering angles.

In the expression for the absolute normalization the ratio V_V/V_{Ne} enters,[17] where V_V (V_{Ne}) is the volume of the vanadium (neon) illuminated by the incident beam and seen by the detector. Besides the trivial effect of the smaller neon volume due to the thickness of the BN disks, we took into account the effect that, seen from the detector, a fraction of the neon sample was screened by the disks. This fraction was 0.034 and 0.047 for the detectors of 20 and 30 cm length, respectively. The "structure factor" of vanadium, including single and multiple elastic scattering, the Debije-Waller factor, and self-shielding, was determined by means of a simulation with MSCAT and decreased monotonically from 0.77 for the smallest to 0.74 for the largest scattering angles. The experimental vanadium spectra were corrected for inelastic scattering as described in Ref. 2.

In order to correct the neon TOF spectra for multiple scattering and duty-cycle overlap, the experiment was simulated by MSCAT. The correction was performed iteratively (cf. Ref. 2). For the first iteration step we used as an input kernel the (scaled) experimental $S(k,\omega)$ of argon at the corresponding thermodynamic state[2] for $k<47$ nm^{-1}, and the large-k Gram-Charlier expansion[19] for $k>47$ nm^{-1}. In the simulation, intensities originating from the following types of scattering could be distinguished: single scattering in the sample (denoted by s), multiple scattering in the sample only (ss) and in both the sample and container, the last collision before detection being in the sample (cs) or in the container (sc). Because of the poor statistical accuracy of the sc intensity the assumption cs=sc was made and 2cs (rather than cs+sc) was used in the correction.[2]

To show the relative importance of the different contributions to the total intensity, the integrated simulated intensities of s, ss, 2cs, and duty-cycle overlap ov (Ref. 2) (mainly determined by neutrons scattered once by the sample) are given in Fig. 3 for measurement 1 as a function of scattering angle. The effect of the BN disks was simulated by taking the total height of the container tubes to be the distance between two disks. In this way the contribution of neutrons scattered first in one tube and then at the same "floor" in the neighboring tube is taken into account, whereas the contribution of the neutrons scattered a second time one floor higher or lower are not. The former contribution was estimated to be 10% of the total

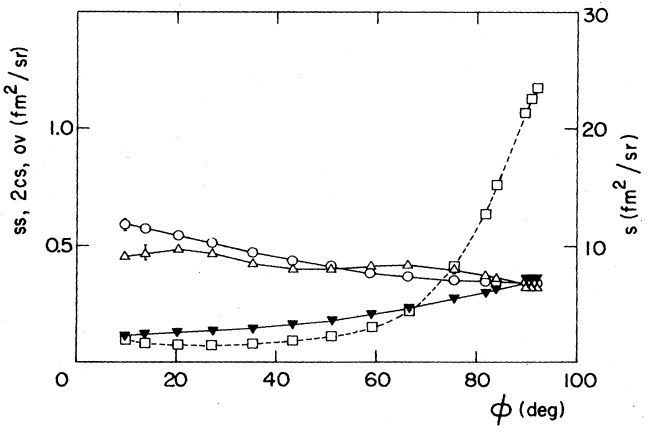

FIG. 3. Integrated intensity from simulation by means of MSCAT of Ne, 35 K, 8 MPa as a function of scattering angle. □, s (right scale); ○, ss; △, 2cs; ▼, ov (left scale).

multiple scattering by comparing the results from two MSCAT runs, one simulating one container tube and one simulating three tubes. The latter contribution was estimated to be 3% of the total multiple scattering intensity (by comparing the solid angle from a section of one tube to the section of a neighboring tube at the same floor with the effective solid angle to a section one floor up or down, taking into account the screening of the BN disks), and was neglected in the correction.

We subtracted the incoherent scattering from the normalized spectra. The intensity was calculated with $\sigma_i = 0.008$ b and the shape was taken equal to the elastic part of the vanadium spectra. For small k, which was the only region where this small correction was significant—the magnitude of the correction in the peak of the spectra was here of the order of the estimated standard deviation—the FWHM of $S_{\text{inc}}(k,\omega)$ is approximately $2Dk^2$. The self-diffusion coefficient D for conditions 1 and 2 is 2.5×10^{-9} and 2.1×10^{-9} m^2 s^{-1}, respectively,[20] resulting in a spectral width smaller than the experimental TOF resolution at scattering angles smaller than 60°.

C. Quality checks

Two relationships are used to check the quality of the fully corrected $S(k,\omega)$ data and the reliability of the estimated standard deviation. The first one is the detailed balance condition which implies that $\tilde{S}(k,\omega)$ is symmetric in ω. For $|\omega| < 5$ ps^{-1} both energy-loss and energy-gain data are available as shown in Fig. 4 for measurement 1. The consistency of these data is quantified by the quality factor $Q(\omega)$.[17,2] If the energy-gain and energy-loss results were normally distributed around $\tilde{S}(k,\omega)$ (which is determined by the weighted mean of the energy-loss and energy-gain data,[17] given by the solid line in Fig. 4) then $Q^2(\omega)$ would follow a χ^2 distribution with one degree of freedom with expectation value 1. $Q(\omega)$ is an indication of the ratio of systematic error (as a result of, e.g., imperfections in the data-reduction procedure) divided by the estimated standard deviation. In Figs. 5(a) and 5(b) $Q(\omega)$ is given for both measurements. For $|\omega| < 4$ ps^{-1} a considerable discrepancy is present (see also Fig. 4). This may be caused by an erroneous correction for background scattering.

The second relationship is the first frequency moment of $S(k,\omega)$ which is exactly known,

$$\int_{-\infty}^{\infty} \omega S(k,\omega) d\omega = \omega_R = \frac{\hbar k^2}{2M} .$$

The ratio of the experimental and exact $\langle\omega\rangle$, $\langle\omega\rangle/\omega_R$, is shown in Figs. 5(c) and 5(d). At small k values only a relatively small ω range is experimentally accessible due to the limited kinematic region covered by the experiment (see Fig. 1). For ω values larger than this limit $\omega_L(k)$ the structured gas model of Sköld[21] was used for the determination of $\langle\omega\rangle$.[17] For $k \geq 12$ nm^{-1} $\omega_L(k)$ was taken to be 15 ps^{-1}. At this frequency the estimated standard deviation of $S(k,\omega)$ was of the order of 100%. The contribution to $\langle\omega\rangle$ of this model is indicated in Figs. 5(c) and 5(d). For $k \gtrsim 10$ nm^{-1} $\langle\omega\rangle$ and ω_R are in good agreement. For $k < 10$ nm^{-1} the contribution of the large-frequency extrapolation is considerable and consequently the calculated $\langle\omega\rangle$ is less reliable.

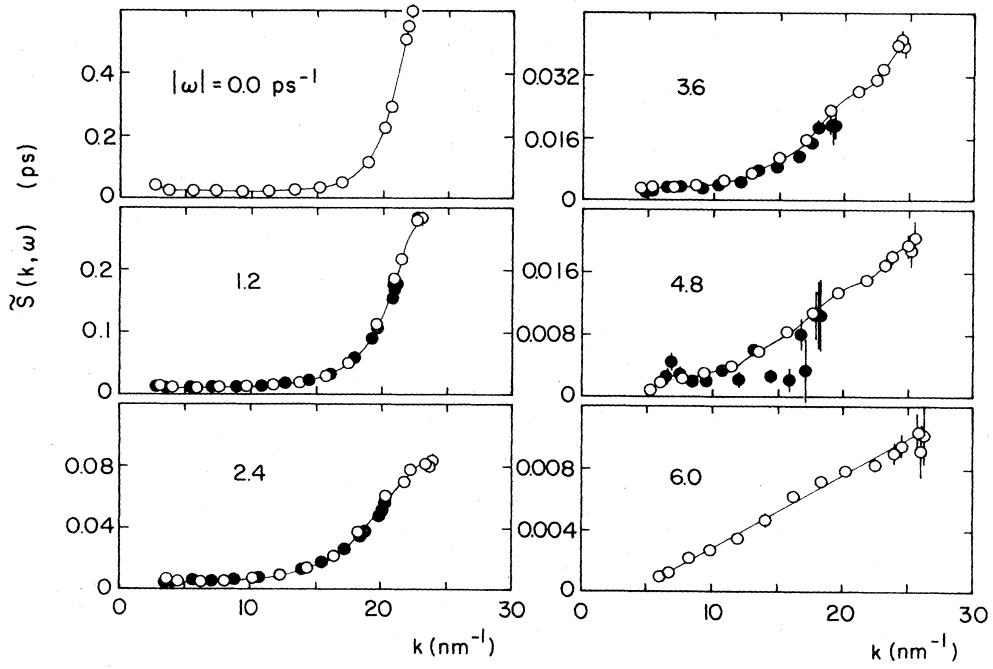

FIG. 4. $\tilde{S}(k,\omega)$ of Ne, 35 K, 8 MPa as a function of k: ○, neutron energy-gain data; ●, energy-loss data; ——, interpolated values for obtaining $\tilde{S}(k,\omega)$ at equidistant k values.

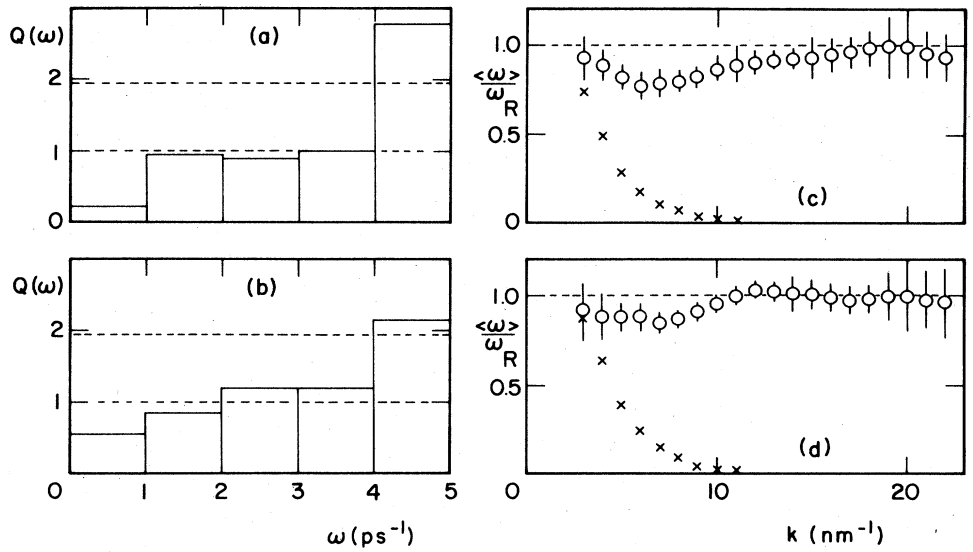

FIG. 5. (a) and (b) Quality factor $Q(\omega)$ for measurements 1 and 2, respectively. Upper 95% limit and the mean of the χ^2 distribution with one degree of freedom are indicated by dashed lines. (c) and (d) Ratio of the experimental and exact first frequency moment for measurements 1 and 2, respectively. Crosses indicate the contribution of the large-frequency extrapolation (see text).

III. RESULTS AND DISCUSSION

A. Static structure factor

$S(k)$ and $\tilde{S}(k)$ were obtained by numerical integration of $S(k,\omega)$ and $\tilde{S}(k,\omega)$, respectively. The contribution of the large-frequency extrapolation (see discussion on $\langle\omega\rangle$ in Sec. II) was smaller than 10% for $k \geq 5$ nm^{-1}, and smaller than 1% for $k \geq 7$ nm^{-1}. In Fig. 6 these $S(k)$'s are plotted together with results from ND of liquid neon[10] and from INS of liquid argon.[2] The reduced temperature of both liquids is 0.97 and the reduced densities $n^* = n\sigma^3$ of neon at 8 and 14 MPa and of argon at 11.5 and 27 MPa are 0.725, 0.752, 0.702, and 0.740, respectively. In Ref. 10 the tabulated ND data had been corrected for a relative incoherent scattering contribution of 0.02. The best value known at present[12] is 0.003(7). In order to obtain results that can be compared with the present INS data we corrected the tabulated values of Ref. 10 by

$$S(k) = \frac{1}{1.017}[S_{\text{tab}}(k) + 0.017] .$$

The neon results of INS and ND agree reasonably well. The correspondence between Ar and Ne is quite good, except for wave numbers in the region around $k^* = 2$ where $S(k)$ of argon is systematically larger. It is unlikely that these differences can be explained on the basis of the quantum nature of neon since when comparing $S(k)$ and $\tilde{S}(k)$ the latter has a tendency to be smaller in this region. It should be noted here, however, that in $\tilde{S}(k)$ only quantum effects of order $\hbar$ are exactly corrected for (see also Sec. III B) and in principle it is possible that the observed differences are caused by effects of order $\hbar^2$ or higher. Other causes for this deviation from CSP might be a different shape of the pair interaction potential (in particular of its attractive part, since the small-k region is sensitive to this part[22]) or differences in the three-particle interactions. When the latter interactions are approximated by the triple-dipole dispersion term, introduced by Axilrod and Teller,[23] its strength is given by ν. For neon and ar-

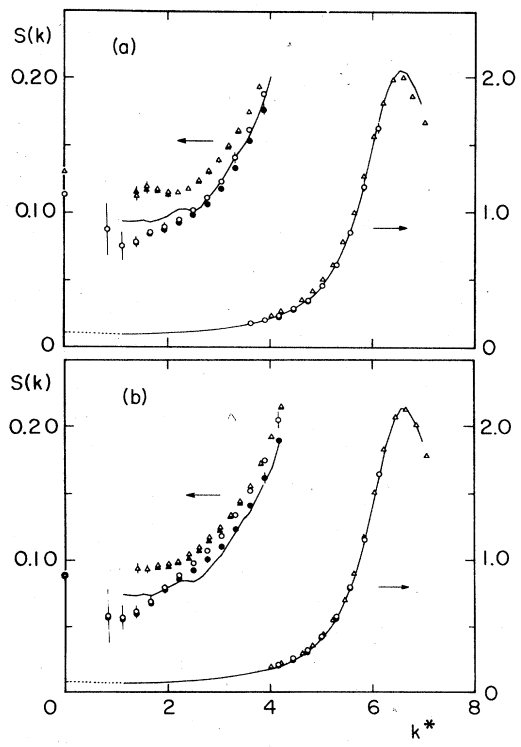

FIG. 6. Static structure factor as a function of $k^* = k\sigma$ of (a) ^{36}Ar, 120 K, 11.5 MPa and Ne, 35 K, 8 MPa, (b) ^{36}Ar, 120 K, 27 MPa and Ne, 35 K, 14 MPa. ——, $S(k)$: neon, ND, Ref. 10. ○, $S(k)$ and ●, $\tilde{S}(k)$: neon, INS, present experiment. △, $S(k)$ and ▲, $\tilde{S}(k)$: argon, INS, Ref. 2. $k^* = 0$ values are calculated from the compressibility.

gon $\nu=1.23\times10^{-5}$ and 5.32×10^{-4} K nm^9,[24] resulting in the dimensionless values $\nu^*=0.033$ and 0.079, respectively. Thus these interactions in argon are about 2.5 times stronger than in neon.

B. The second frequency moment and quantum effects

The nth frequency moment of $S(k,\omega)$ is defined by

$$\langle\omega^n\rangle=\int_{-\infty}^{\infty}\omega^n S(k,\omega)d\omega$$

and its quasiclassical approximation by

$$\langle\tilde{\omega}^n\rangle=\int_{-\infty}^{\infty}\omega^n\tilde{S}(k,\omega)d\omega\ .$$

For a monatomic, mono-isotopic system with pairwise additive interaction potential $u(r)$, $\langle\omega^n\rangle$ for $n=2$ and 4 is given by[25]

$$\langle\omega^2\rangle=\frac{k^2}{\beta M}\left[1+\frac{\hbar^2\beta}{4M}k^2+\frac{\hbar^2\beta^2}{12}[\Omega^2(0)-\Omega^2(k)]+O(\hbar^4)\right], \tag{4}$$

where

$$\Omega^2(k)=\frac{n}{M}\int d^3r\, g(r)\cos(kz)\frac{d^2u(r)}{dz^2}\ ,$$

and

$$\langle\omega^4\rangle=\frac{k^2}{\beta M}\left[\frac{3k^2}{\beta M}+\Omega^2(0)-\Omega^2(k)\right]+O(\hbar^2)\ . \tag{5}$$

If the sample consists of more than one isotope Eqs. (4) and (5) should be modified according to Fredrikze.[25] In the present case these corrections are negligibly small. Making use of the detailed-balance condition [Eq. (2)] the symmetric part of $S(k,\omega)$ is defined by

$$S_{\rm sym}(k,\omega)=\tfrac{1}{2}[S(k,\omega)+S(k,-\omega)]=\tfrac{1}{2}(1+e^{-\beta\hbar\omega})S(k,\omega).$$

The quasiclassical approximation $\tilde{S}(k,\omega)$ [Eq. (3)] is related to $S_{\rm sym}(k,\omega)$ by

$$\tilde{S}(k,\omega)=\exp\left[\frac{-\hbar^2k^2\beta}{8M}\right]\mathrm{sech}(\tfrac{1}{2}\beta\hbar\omega)S_{\rm sym}(k,\omega)\ . \tag{6}$$

Series expansion in $\hbar^2$ yields an expression for the quasiclassical second frequency moment $\langle\tilde{\omega}^2\rangle$ in terms of the real frequency moments:

$$\langle\tilde{\omega}^2\rangle=\int_{-\infty}^{\infty}\omega^2\left[1+\hbar^2\left[\frac{\beta k^2}{8M}-\frac{\beta^2\omega^2}{8}\right]+O(\hbar^4)\right]S_{\rm sym}d\omega$$

$$=\langle\omega^2\rangle+\frac{\hbar^2\beta k^2}{8M}\left[\langle\omega^2\rangle-\frac{\beta M}{k^2}\langle\omega^4\rangle\right]+O(\hbar^4)\ . \tag{7}$$

Inserting the expressions for $\langle\omega^2\rangle$ and $\langle\omega^4\rangle$ [Eqs. (4) and (5)] yields

$$\langle\tilde{\omega}^2\rangle=\frac{k^2}{\beta M}\left[1-\frac{\hbar^2\beta^2}{24}[\Omega^2(0)-\Omega^2(k)]\right]+O(\hbar^4)\ . \tag{8}$$

The deviation of the second frequency moment $\langle\omega^2\rangle$ from the classical one, $\langle\omega^2\rangle_{\rm cl}=k^2(\beta M)^{-1}$, consists—to order $\hbar^2$—of two terms [Eq. (4)]. One term is proportional to k^2 and can be calculated exactly, the second depends on $g(r)$ and $u(r)$.

In the quasiclassical approximation $\langle\tilde{\omega}^2\rangle$, the term $\sim k^2$ cancels and the second term is reduced by a factor of 2 and also changes sign. Note that in the approximation $\tilde{S}(k,\omega)$ [Eq. (3)] quantum effects of order $\hbar^2$ are still present.

We calculated $\Omega^2(k)$ for a LJ system with $n^*=0.702$ and $T^*=0.974$ according to the mean spherical approximation (MSA),[26] which is consistent with $\Omega^2(k)$ obtained from neutron scattering results of argon and from the second time derivative of the longitudinal current correlation function obtained in a CMD simulation for a LJ system.[2] Results for $\langle\omega^2\rangle$ and $\langle\tilde{\omega}^2\rangle$ from these calculations and from the experiments are shown in Fig. 7 for both argon and neon. Within the relatively large uncertainties the experimental data are in agreement with the calculation.

In general, quantum corrections are expected to be negligible if two conditions are satisfied. (i) The length scale, relevant to the observed quantity, is large compared with the thermal de Broglie wavelength $\lambda_T=\hbar(2\pi\beta/M)^{1/2}$ or equivalently $k\ll k_q=2\pi/\lambda_T$. (ii) The relevant time scale is large compared with $\hbar\beta$, or $\omega\ll\omega_q=(\hbar\beta)^{-1}$. If the de Boer parameter $\Lambda^*=2\pi\hbar\sigma^{-1}(M\varepsilon)^{-1/2}$ (which is proportional to $\lambda_T^*=\lambda_T\sigma^{-1}$ at $T^*=k_BT/\varepsilon=1$) is used as a measure of the quantum nature of a LJ system then

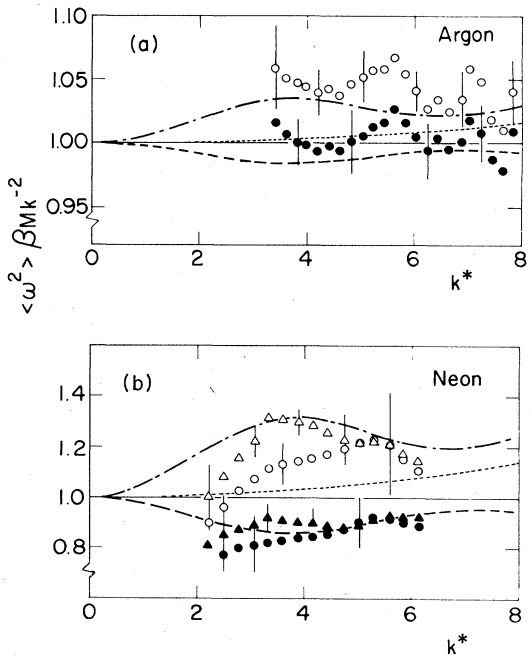

FIG. 7. Second frequency moment of $S(k,\omega)$ divided by its classical value. (a) ○, $\langle\omega^2\rangle\beta Mk^{-2}$ and ●, $\langle\tilde{\omega}^2\rangle\beta Mk^{-2}$: ^{36}Ar, 120 K, 11.5 MPa, Ref. 2. (b) ○, $\langle\omega^2\rangle\beta Mk^{-2}$ and ●, $\langle\tilde{\omega}^2\rangle\beta Mk^{-2}$, for Ne, 35 K, 8 MPa; △, $\langle\omega^2\rangle\beta Mk^{-2}$ and ▲, $\langle\tilde{\omega}^2\rangle\beta Mk^{-2}$, for Ne, 35 K, 14 MPa. —·—·—·, calculated $\langle\omega^2\rangle\beta Mk^{-2}$ [Eq. (4)]; · · ·, k^2 contribution to $\langle\omega^2\rangle\beta Mk^{-2}$; — — —, calculated $\langle\tilde{\omega}^2\rangle\beta Mk^{-2}$ [Eq. (8)].

TABLE IV. Quantum parameters. λ_T^*, ω_q^*, and k_q^* are calculated for argon and neon at 120.0 and 35.08 K, respectively.

	^{36}Ar	Ne
Λ^*	0.196	0.580
λ_T^*	0.079	0.235
ω_q^*	32	11
k_q^*	80	27

$$k_q^* = k_q\sigma = (2\pi)^{3/2}(\Lambda^*)^{-1}(T^*)^{1/2}$$

and

$$\omega_q^* = \omega_q\tau = 2\pi(\Lambda^*)^{-1}T^*$$

apply. The values of these quantities for the present thermodynamic conditions are listed in Table IV. In the k range studied here condition (i) is satisfied for both argon and neon. However, even at these relative small k values the quantum corrections to $\langle\omega^2\rangle$ appear to be considerable (up to 20%) for neon. This is a consequence of the fact that condition (ii) is not satisfied, since the frequencies relevant to $\langle\omega^2\rangle$ are of the order of ω_m where $\omega^2 S(k,\omega)$ has its maximum (Sec. III C). For instance, ω_m^* at $k^*=4$ is found to be equal to 15, which is of the same order of magnitude as ω_q^* for neon.

If Eq. (4) is reduced by means of the parameters σ, ε, and M it is readily shown that, at fixed T^*, the corrections of order $\hbar^2$ are proportional to $(\Lambda^*)^2$, implying that the quantum corrections to $\langle\omega^2\rangle$ and $\langle\tilde{\omega}^2\rangle$ of neon are a factor of 9 larger than those of argon (see Table IV and Fig. 7).

C. Dynamic structure factor, short-wavelength heat and sound modes

According to kinetic theory for a classical system[5] $S(k,\omega)$ can be decomposed into an infinite sum of "Lorentzians"

$$S(k,\omega) = \frac{1}{\pi}\mathrm{Re}F(k,z=i\omega)\ , \tag{9}$$

$$F(k,z) = S(k)\sum_{j=-\infty}^{\infty}\frac{A_j(k)}{z+z_j(k)}\ , \tag{10}$$

where $F(k,z)$ is the Laplace transform of the intermediate scattering function $\hat{F}(k,t)$. The parameters A_j and z_j are either real or appear as conjugate pairs and obey sum rules following from the short-time behavior of $\hat{F}(k,t)$:

$$\sum_{j=-\infty}^{\infty}A_j(k)[z_j(k)]^n = R_n(k)\ , \tag{11}$$

with

$$R_0(k)=1,\ R_1(k)=0\ ,$$

$$R_2(k) = -\omega_0^2 = -\frac{k^2}{\beta MS(k)} = -\langle\omega^2\rangle/\langle\omega^0\rangle\ , \tag{12}$$

$$R_3(k)=0,\ R_4(k)=\omega_0^2\omega_l^2=\langle\omega^4\rangle/\langle\omega^0\rangle\ ,$$

where $\omega_l^2 = 3k^2(\beta M)^{-1}+\Omega^2(0)-\Omega^2(k)$.

In the hydrodynamic limit ($k\to 0$) the infinite sum of Eq. (10) reduces to a sum of three Lorentzians [Eq. (1)], representing one heat mode ($j=0$) and two sound modes ($j=\pm 1$). If we define the quantities $R_n'(k)$ for this truncated sum analogous to Eq. (11), then in this limit $R_n'(k)=R_n(k)$ for $n=0$, 1, and 2, and the third and higher sum rules are violated, i.e., $R_n'(k)\neq R_n(k)$ for $n\geq 3$ (see Appendix).

In order to interpret our experimental data in terms of extended heat and sound modes, as discussed in the Introduction, the three-pole (TP) approximation Eq. (1) was fitted to the $\tilde{S}(k,\omega)$ data by means of a weighted least-squares method. Two cases are distinguished: model TP1, imposing the restrictions $R_n'(k)=R_n(k)$ for $n=0$ and $n=1$; and model TP2 with the restrictions $R_n'(k)=R_n(k)$ for $n=0$, 1, and 2. Model TP2 has four free parameters, viz., $S(k)$, $z_{-1}(k)$, $z_0(k)$, and $z_{+1}(k)$, and in model TP1 $\omega_0^2(k)$ may be considered as an additional free parameter. For each k we determined the mean-square deviation

$$\delta^2(k) = \frac{1}{N-p}\sum_{i=1}^{N}\frac{[f_i-\tilde{S}(k,\omega_i)]^2}{\sigma_i^2}\ , \tag{13}$$

with N the number of discrete data points $\tilde{S}(k,\omega_i)$ at a particular k value, σ_i the estimated standard deviation, and f_i the value at ω_i of the fitted model. As a consequence of the correction procedure the experimental data are correlated,[17] and $(N-p)\delta^2(k)$ will not follow a χ^2 distribution. Since these correlations will in general be positive, values of $\delta(k)$ smaller than 1 are very well possible.

Both models TP1 and TP2 gave excellent fits with $\delta(k)<1$ for all k values. In Fig. 8 the results of measure-

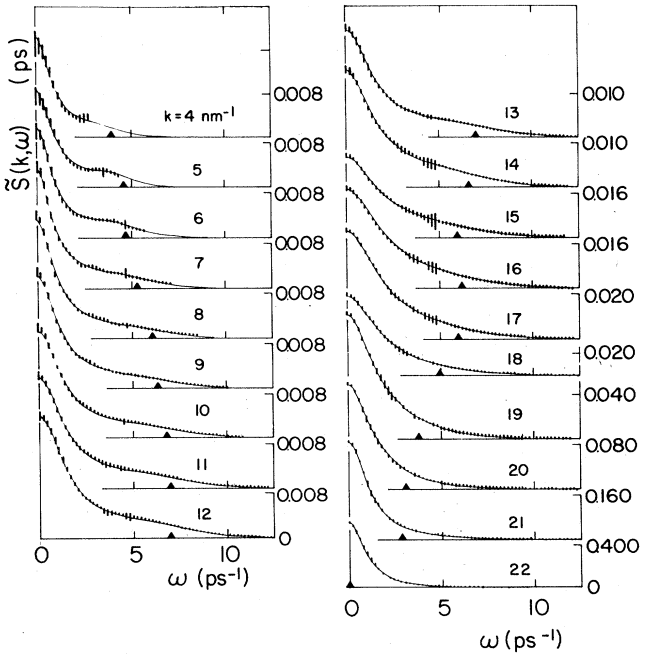

FIG. 8. Fully corrected $\tilde{S}(k,\omega)$ of measurement 2—Ne, 35 K, 14 MPa—(error bars) and model TP2 (solid line). Sound frequencies $\omega_s(k)=\mathrm{Im}z_{+1}(k)$ are indicated by the triangles.

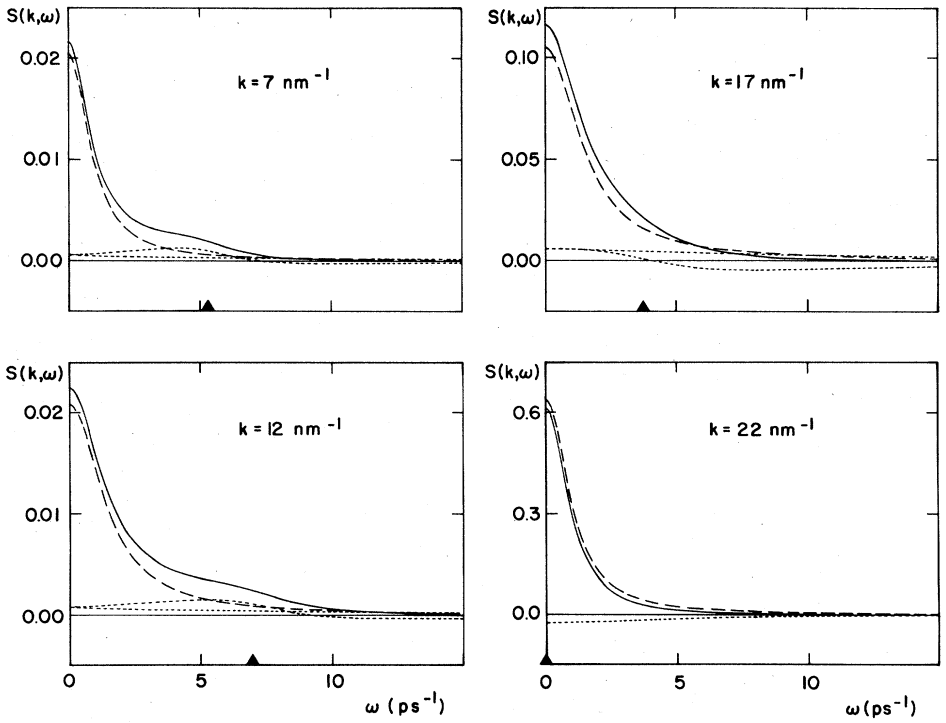

FIG. 9. Decomposition of $\tilde{S}(k,\omega)$ of measurement 2 into its eigenmodes. Solid line, best fit (same as Fig. 8); dashed line, (extended) heat mode; dotted lines, left and right (extended) sound modes; triangle, sound frequency $\omega_s(k)$. N.B. Intensity of the second (central) sound mode at $k=22$ nm^{-1} is negligible.

ment 2 and the best fit of model TP2 are displayed. Except for some values of k around $k=20$ nm^{-1} (where z_j and A_j are real) $z_{\pm1}(k)$ and $A_{\pm1}(k)$ appear as conjugate pairs yielding the Rayleigh-Brillouin triplet

$$\frac{S(k,\omega)}{S(k)}=\frac{A_0}{\pi}\frac{z_0}{\omega^2+z_0^2}+\frac{A_s}{\pi}\left[\frac{z_s+(\omega+\omega_s)\tan\varphi}{(\omega+\omega_s)^2+z_s^2}+\frac{z_s-(\omega-\omega_s)\tan\varphi}{(\omega-\omega_s)^2+z_s^2}\right] \tag{14}$$

with heat damping z_0, sound damping $z_s=\mathrm{Re}z_{\pm1}$, sound frequency $\omega_s=\mathrm{Im}z_{+1}$, $A_s=\mathrm{Re}A_{\pm1}$, and $\tan\varphi=(\mathrm{Im}A_{+1})/A_s$.

In Fig. 9 the decomposition of $S(k,\omega)$ into the heat and sound modes is indicated for some representative k values. It appears that—in the k range studied—the behavior of three eigenmodes can very well describe the dramatic change in shape of $S(k,\omega)$ as a function of k (see Fig. 8). There is no distinct maximum in $S(k,\omega)$ at $\omega\neq0$ (as is the case in the hydrodynamic limit) but a shoulder is visible at the smaller k values. For increasing k this shoulder becomes less pronounced, shifts to larger ω, and disappears gradually as k approaches 22 nm^{-1}. This change in shape can be understood as a manifestation of the short-wavelength sound modes.

In order to test CSP for the dynamic behavior of neon and argon we proceed as follows. First we compare the bare experimental results and some derived quantities and then the interpretation in terms of the eigenmodes is discussed. In Fig. 10 $\tilde{S}(k,\omega)[\tilde{S}(k)\tau]^{-1}$ is shown for argon and neon. The argon data are represented by a continuous line and the estimated uncertainties are approximately a factor of 2 smaller than the corresponding neon values (see Ref. 2). Note that at small values of k^* the experi-

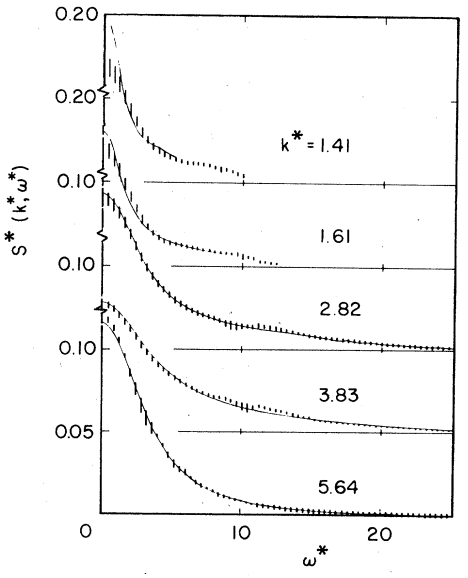

FIG. 10. Reduced dynamic structure factor $S^*(k,\omega)=\tilde{S}(k,\omega)[\tilde{S}(k)\tau]^{-1}$, for five representative k^* values. Error bars, neon measurement 1 ($T^*=0.969$, $n^*=0.725$); solid line, argon measurement b of Ref. 2 ($T^*=0.974$, $n^*=0.702$).

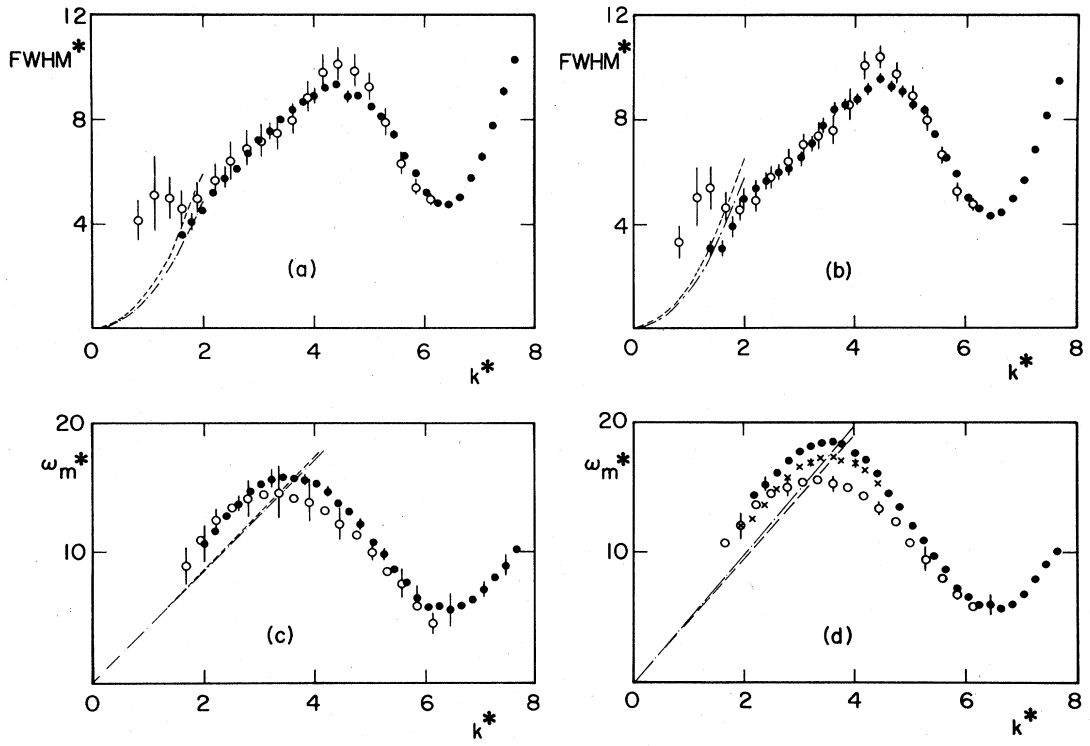

FIG. 11. Reduced full width at half maximum of $\tilde{S}(k,\omega)$ (FWHM*=FWHMτ) as a function of $k^*=k\sigma$. (a) circles, neon measurement 1 ($T^*=0.969$, $n^*=0.725$); dots, argon measurement b of Ref. 2 ($T^*=0.974$, $n^*=0.702$). (b) circles, neon measurement 2 ($T^*=0.969$, $n^*=0.752$); dots, argon measurement c of Ref. 2 ($T^*=0.974$, $n^*=0.740$). Reduced peak position of the longitudinal current correlation function $\tilde{C}_l(k,\omega)$, $\omega_m^*=\omega_m\tau$, as a function of k^*: (c) key as in (a); (d) key as in (b); crosses, redetermined values of argon (see text). Dashed and dash-dotted lines represent the hydrodynamic limits for neon and argon, respectively.

mentally accessible ω^* range is larger in the case of neon (see also Fig. 1). In Figs. 11(a) and 11(b) the full width at half maximum (FWHM) of $\tilde{S}(k,\omega)$ is given. For $k^*\lesssim 1.5$ the FWHM of neon is too large compared to both the hydrodynamic value $2ak^2$ (Table V) and the corresponding argon results. Probably this is caused by incorrect subtraction of the background scattering at the smaller scattering angles resulting in a too low intensity around $\omega=0$ (see $k^*=1.4$ in Fig. 10). For $2\lesssim k^*\lesssim 6$ the FWHM's of argon and neon agree very well.

In Figs. 11(c) and 11(d) the peak position ω_m of the longitudinal current correlation function $\tilde{C}_l(k,\omega)$

TABLE V. Thermodynamic and transport properties (from Ref. 15).

		Measurement 1	Measurement 2
Spec. heat const. pressure	c_p (10^{-23} J K^{-1})	6.5(2)	6.2(2)
Spec. heat const. volume	c_v (10^{-23} J K^{-1})	2.9(2)	3.1(2)
	$\gamma=c_p/c_v$	2.23(8)	1.98(6)
Structure factor at $k=0$[a]	$S(0)$	0.115	0.089
Adiabatic sound velocities[b]	c_s (m s^{-1})	530	570
Shear viscosity	η (10^{-5} kg m^{-1} s^{-1})	8.4(3)	9.3(3)
Thermal conductivity	λ (10^{-1} W m^{-1} K^{-1})	1.09(3)	1.19(3)
Thermal diffusivity[c]	a (10^{-8} m^2 s^{-1})	5.0(2)	5.6(2)
Sound damping factor[d]	Γ (10^{-8} m^2 s^{-1})	12	12
Longitudinal viscosity[d]	Φ (10^{-8} m^2 s^{-1})	18	19

[a] $S(0)=k_BT(\partial n/\partial p)_T$.
[b] $c_s^2=\gamma[\beta MS(0)]^{-1}$.
[c] $a=\lambda(nc_p)^{-1}$.
[d] From argon data (Ref. 27), scaled to neon; $\Gamma=\frac{1}{2}[\Phi+(\gamma-1)a]$. Dimensionless values are defined by $c_s^*=(M/\varepsilon)^{1/2}c_s$, $\eta^*=\sigma(M\varepsilon)^{-1/2}\eta$, $\lambda^*=k_B^{-1}(M/\varepsilon)^{1/2}\lambda$, $a^*=\sigma^{-1}(M/\varepsilon)^{1/2}a$, $\Gamma^*=\sigma^{-1}(M/\varepsilon)^{1/2}\Gamma$.

$=\omega^2\tilde{S}(k,\omega)/k^2$ is shown. Since some doubt exists about the ω_m results for $k^* \lesssim 4$ of argon at 27 MPa (Ref. 2) we redetermined these by interpolating the ω_m data at 2, 11.5, and 40 MPa. These new values are indicated by crosses in Fig. 11(d). Again the overall agreement between neon and argon is good. However, the neon values in the neighborhood of the maximum of $\omega_m(k)$ are systematically somewhat smaller.

In Fig. 12 three parameters obtained from fits of the three-pole model [Eq. (1)] to the data are shown as a function of k. The error bars connect the values obtained using models TP1 and TP2. The hydrodynamic limits $z_0=ak^2$, $z_s=\Gamma k^2$, and $\omega_s=c_s k$ (Table V for neon and Ref. 2 for argon) are indicated. At k values around $k^*=6$ the best fit is accomplished with three (different) real poles (i.e., $\omega_s=0$). In these cases the strength of one of the overdamped sound modes, say A_{+1}, of neon is too weak to be detected and only the decay constant of the other sound mode, z_{-1}, is displayed.

The neon and argon[3] results have the same features. (i) z_0 is about one-half the FWHM. The width of $\tilde{S}(k,\omega)$ is mainly determined by the heat mode. (ii) A sound propagation gap, indicating overdamped sound modes, is present near the main peak in $S(k)$. (iii) Except in the region in and around the gap ω_s and ω_m behave very similarly. This is in agreement with the observation[4] that $C_l(k,\omega)$ is largely determined by the sound modes. (iv) ω_s exhibits anomalous dispersion (i.e., with decreasing k ω_s approaches its hydrodynamic limit from above) which has been shown to be consistent with the mode-coupling theory.[28]

The quantitative agreement of z_0, z_s, and ω_s between argon and neon is found to be satisfactory, except for ω_s in the range $3 \lesssim k^* \lesssim 5$. In this region the ω_s values of neon are smaller than those of argon, which is consistent with the ω_m results (Fig. 11). It is not clear whether the differences in ω_s and ω_m between neon and argon may be considered significant. Also, the question of what may be the origin of these differences is still open.

D. Generalized hydrodynamics description

The fact that $S(k,\omega)$ can well be described by a three-pole approximation, as was shown in Sec. III C, implies that $S(k,\omega)$ may be considered a solution of the linearized hydrodynamic equations containing k-dependent thermodynamic and transport coefficients. The interpretation of $S(k,\omega)$ in terms of generalized hydrodynamics has been

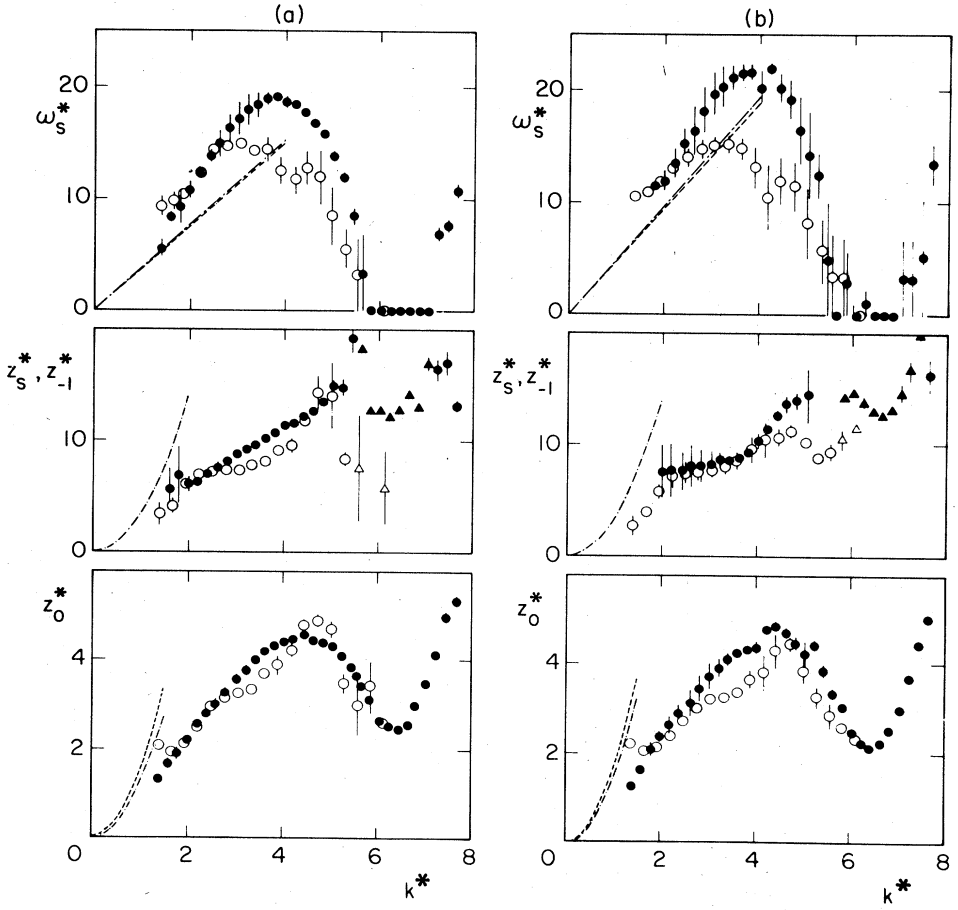

FIG. 12. Sound frequency $\omega_s^*=(\mathrm{Im}z_{+1})\tau$ and decay constants $z_0^*=z_0\tau$ and $z_s^*=(\mathrm{Re}z_{\pm1})\tau$ of the heat and sound modes, respectively, as a function of $k^*=k\sigma$: (a) key as in Fig. 11(a); (b) key as in Fig. 11(b). In the case of overdamped sound modes ($\omega_s=0$) only one decay constant, z_{-1}, is shown (triangles).

applied by Bell *et al.*[8] and by Lonngi and Garcia-Colin[29] to results for neon near the triple point from two sets of INS data.[8,30] In both interpretations a k dependence of the transport coefficients and subsequently an additional frequency dependence are introduced.

The solution of the linearized Navier-Stokes equations for the density-density correlation function in Laplace space is[31]

$$F(k,z)=S(0)\left[z+\frac{\omega_0^2}{z+z_\Phi+\dfrac{(\gamma-1)\omega_0^2}{z+z_T}}\right]^{-1} \tag{15}$$

with $\omega_0^2=\gamma^{-1}c_s^2k^2$, $S(0)=\beta^{-1}(\partial n/\partial p)_T$, $z_\Phi=\Phi k^2$, and $z_T=D_Tk^2$. Of the three thermodynamic quantities γ, $S(0)$, and c_s, only two are independent due to the relation $S(0)=\gamma(\beta Mc_s^2)^{-1}$. The two transport coefficients in this description are the longitudinal viscosity $\Phi=(\zeta+\frac{4}{3}\eta)/(nM)$, and $D_T=\lambda/(nc_v)=\gamma a$, with a the thermal diffusivity (Table V). Note that Eq. (15) obeys the first three sum rules, $R_n'(k)=R_n(k)$, $n=0$, 1, and 2 (see Appendix).

Mountain derived a generalization of Eq. (15), Eq. (2.40) in Ref. 31(a), employing the memory-function formalism developed by Mori.[32] As a result the transport coefficients become k- and z-dependent, yielding $z_\Phi(k,z)$ and $z_T(k,z)$, which are memory functions associated with current and heat fluxes, respectively. The term $(\gamma-1)\omega_0^2$ is then replaced by a complicated function of both static and dynamic quantities. The static quantities are the generalizations of c_v and $(\partial p/\partial T)_n$, involving static correlations among three and four particles. The dynamic quantities $z_{\Phi T}(k,z)$ and $z_{T\Phi}(k,z)$ are memory functions which describe the coupling between the current and heat fluxes. Furthermore, $S(0)$ is replaced by the static structure factor $S(k)$.

If we now make the assumption that the memory functions z_Φ, z_T, $z_{\Phi T}$, and $z_{T\Phi}$ decay on a time scale much shorter than the decay of $\hat{F}(k,t)$ these may be replaced by δ functions in time and thus by a constant in Laplace space. Then we end up with the k-dependent variables $z_\Phi(k)$, $z_T(k)$, and $\gamma(k)$ and Mountain's generalization of Eq. (15) (Ref. 31) will again have three poles and can be identified with Eq. (1). This special case of Mountain's generalization will be referred to as the "generalized hydrodynamics representation" of the three-pole model in the remainder of this paper. If all frequencies are scaled with the k-dependent characteristic frequency $\omega_0=[\beta MS(k)]^{-1/2}k$, the square root of the normalized second frequency moment, the generalized hydrodynamics representation reads

$$\bar{F}(k,\bar{z})=S(k)\left[\bar{z}+\frac{1}{\bar{z}+\bar{z}_\Phi(k)+\dfrac{\gamma(k)-1}{\bar{z}+\bar{z}_T(k)}}\right]^{-1}, \tag{16}$$

where $\bar{F}=F\omega_0$, $\bar{z}=z/\omega_0$, etc.

The relations between $\bar{z}_\Phi(k)$, $\bar{z}_T(k)$, and $\gamma(k)$ in Eq. (16) and $z_{-1}(k)$, $z_0(k)$, and $z_{+1}(k)$ in Eq. (1) are given in Eq. (A14). The hydrodynamic limits of $\bar{z}_\Phi$ and $\bar{z}_T$ are $\gamma^{1/2}\Phi c_s^{-1}k$ and $\gamma^{3/2}ac_s^{-1}k$, respectively.

We will consider three models that were used to fit to the experimental data. First the models TP1 and TP2, already discussed in Sec. III C. These have the free parameters $S(k)$, $z_0(k)$, and $z_{\pm1}(k)$ or, alternatively, $S(k)$, $z_\Phi(k)$, $z_T(k)$, and $\gamma(k)$, where in model TP1 $\omega_0(k)$ is an additional free parameter. In a third model, denoted by TP3, $\gamma(k)$ is kept fixed and taken equal to its hydrodynamic value. Model TP3 was used by Lonngi and Garcia-Colin (model CH in Ref. 29) and by Bell *et al.* (Fig. 8 in Ref. 8). Since the trivial temperature effect (determined by the thermal velocity of the particles which is proportional to $T^{1/2}$) is eliminated by scaling with ω_0, the values from Refs. 8 and 29 may be compared with the present results. The parameters, determined by weighted least-squares fitting, are given in Fig. 13(a) in the three-mode representation and in Fig. 13(b) in the generalized hydrodynamics representation. The root-mean-square deviation of the fit, $\delta(k)$, is defined by Eq. (13). The experiments in Refs. 8 and 29 have been performed at $T=26.5$ K and $n=36.0$ nm^{-3}. The thermodynamic and transport properties at this condition are[8] $\gamma=2.1$, $c_s=600$ m s^{-1}, $D_T=10.5\times10^{-8}$ m^{2}s^{-1}, and $\Phi=21\times10^{-8}$ m^{2}s^{-1}. In Ref. 8 the k range covered was $4<k<14$ nm^{-1} and here we show results from Ref. 29 for $8\leq k\leq22$ nm^{-1}.

E. Discussion

In this paper two representations of $S(k,\omega)$ are discussed. One is the description of the decay of the density fluctuations in terms of the decay of its eigenmodes.[3–7] The second one is the description of $S(k,\omega)$ in terms of k- and ω-dependent transport coefficients.[31] The question which of the two representations exhibits more "physical significance" is still a controversial subject (see, e.g., Refs. 33 and 34). Because of the lack of useful criteria we will not discuss this question but will restrict ourselves to the investigation of the parameters appearing in both representations. In order to have a correct description for all k and ω the infinite series in Eq. (10) as well as both k and ω dependence of the transport coefficients are required. If, however, the hydrodynamic limit $k\rightarrow0$ is considered three Lorentzians suffice, the parameters of which are directly connected with the transport coefficients, and, in the other representation, Eq. (15) holds. As the wave number of the density fluctuations increases the accuracy of the hydrodynamic description decreases. This is because short-range space and time correlations, which are important in the region probed by neutron scattering, are not built into the equations of linearized hydrodynamics. This means that in this k region the three most important eigenmodes will not follow their hydrodynamic values, and higher modes will become more important. Alternatively, it results in a k and ω dependence of the transport coefficients in the second representation. From calculations for a hard-sphere system, using a revised Enskog theory,[5–7] it has been shown that for k values smaller than the inverse mean free path l^{-1} (for the present conditions $l\approx0.03$ nm), $S(k,\omega)$ is mainly determined by the three lowest eigenmodes, and the contribution of the higher modes only influences the high-frequency part of $S(k,\omega)$, which exhibits relatively large experimental uncertainty. This observation is analogous to the assertion

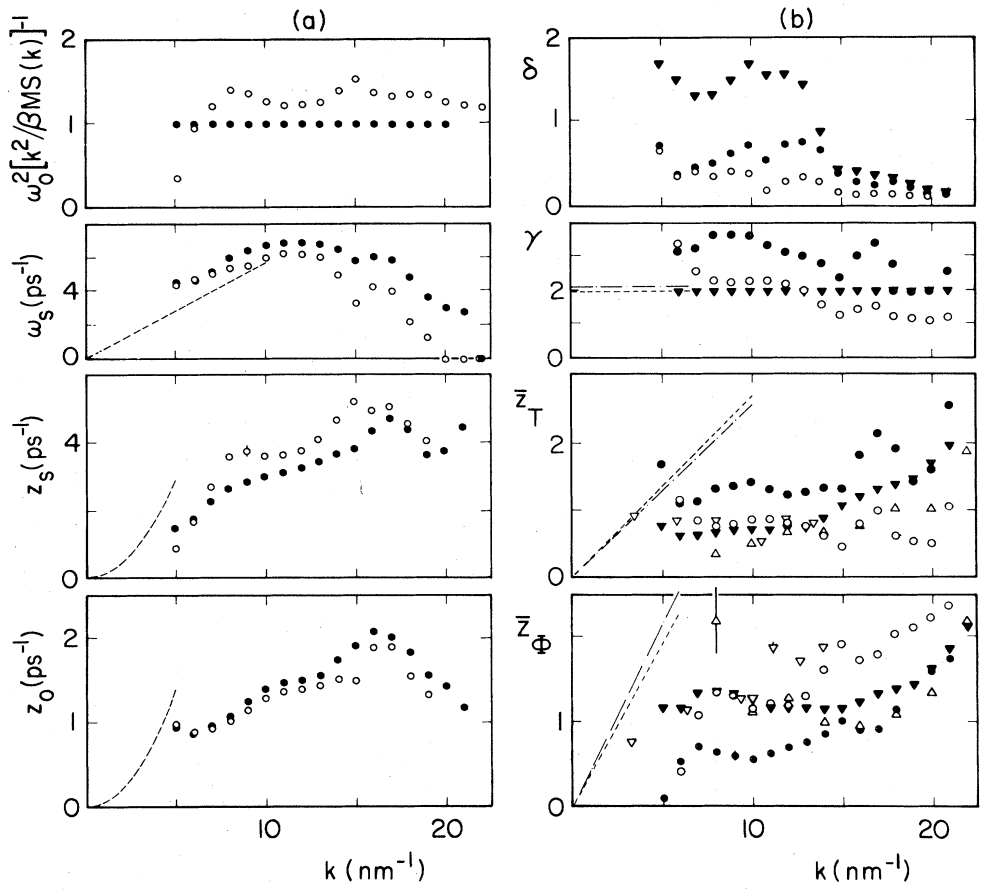

FIG. 13. Parameters of the models TP1 (open circles), TP2 (closed circles), and TP3 (closed triangles) from fits to the experimental $\tilde{S}(k,\omega)$ data of neon at 35 K and 14 MPa, in the three-mode representation [parameters z_0, z_s, and ω_s in (a)] and the generalized hydrodynamic representation [parameters $\bar{z}_\Phi$, $\bar{z}_T$, and γ in (b)]. $\delta(k)$ is the root-mean-square deviation of the fit and ω_0^2 the normalized second frequency moment of the model. Results of model TP3 from neon near the triple point are indicated by ∇ (Ref. 8) and $\triangle$ (Ref. 29). Dashed and dash-dotted lines in (b) indicate the hydrodynamic limits in neon at 35 K and 14 MPa, and at 26.5 K and vapor pressure, respectively.

that the decay as a function of frequency of the generalized transport coefficients is much slower than the decay of $S(k,\omega)$ and will therefore become manifest at larger frequencies.

The aim of this study is to investigate whether a good description of the experimental data can be achieved if only the first three modes are considered or alternatively only k dependence of the transport coefficients is taken into account. In this case the two models can be translated into each other straightforwardly as shown in the Appendix. Note that if more modes are considered and the frequency dependence of the transport coefficients is taken into account this translation is much more complicated.

Both the higher modes and the ω dependence of the transport coefficients are more important with increasing frequency, so, by neglecting these, we may not expect the model to obey all the sum rules. In model TP1 only the first sum rule is satisfied, resulting in five free parameters, whereas in TP2 the first and second sum rules are satisfied, as is the case in the hydrodynamic regime, resulting in four free parameters. From the fits it is apparent that with only four (k-dependent) parameters the present results can be described excellently. Introducing one extra parameter (model TP1) does not improve the fits significantly and introduces correlations among the fitting parameters. We will come back to this below. In model TP3 the number of free parameters is reduced to three. This is accomplished by taking, in the generalized hydrodynamics representation, $\gamma(k)$ equal to its hydrodynamic value. Although, as far as we know, no physical justification exists for the assumption that the k dependence of $\gamma(k)$ is weaker than that of, e.g., $\Phi(k)$ or $D_T(k)$, we will consider this model in order to be able to compare our results with those in Refs. 8 and 29.

The k-dependent transport coefficients $D_T(k) = \omega_0 \bar{z}_T k^{-2}$ and $\Phi(k) = \omega_0 \bar{z}_\Phi k^{-2}$ divided by their hydrodynamic values, and corresponding with the results shown in Fig. 13(b), are displayed in Fig. 14. As found before,[8,29] these quantities decrease with increasing k. The physical meaning of the k dependences of Φ and D_T as well as $\bar{z}_\Phi$, $\bar{z}_T$, and γ is a subject for future study.

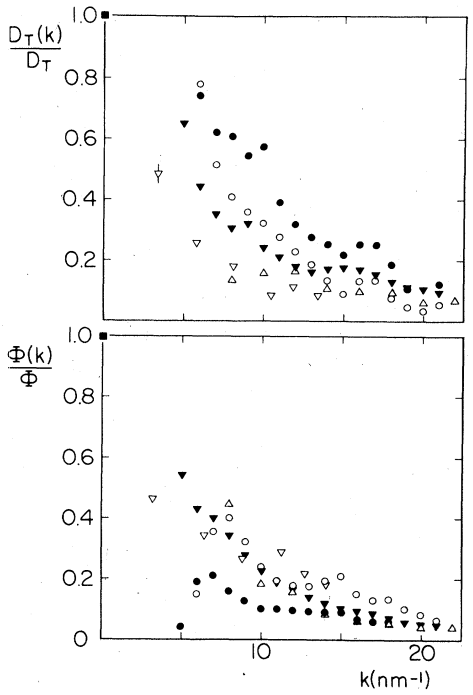

FIG. 14. k-dependent generalized transport coefficients divided by their hydrodynamic values. Key as in Fig. 13.

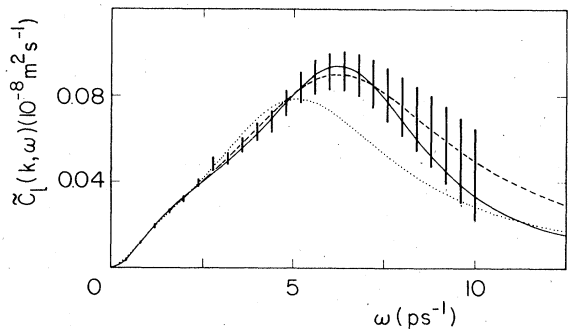

FIG. 15. Experimental data for the longitudinal current correlation function $\tilde{C}_l(k,\omega)=\omega^2\tilde{S}(k,\omega)/k^2$ of neon at 35 K and 14 MPa at wave number $k=9$ nm^{-1} (error bars), and the best fit from the models TP1 (dashed line), TP2 (solid line), and TP3 (dotted line).

From the present results we conclude the following. (i) Both models TP1 and TP2 give a good description of the experimental data. This means that if the requirement that $S(k,\omega)$ has to obey the sum rules higher than the second one is abandoned, which is obviously justified by the uncertainty of the present high-energy data, four parameters are sufficient for the characterization of $S(k,\omega)$. Model TP3 appears to be inadequate for $k \lesssim 15$ nm^{-1}. An example of all three models is given in Fig. 15. (ii) The lowest k value covered by the experiment is too large to see the transition to the hydrodynamic region, which is estimated to extend up to roughly $k=2$ nm^{-1}. However, if the values obtained at $k=5$ nm^{-1} are excluded (at the smaller k values a systematic error might be present in the experimental results, see Sec. II) the parameters in both Figs. 13 and 14 can be extrapolated smoothly to their hydrodynamic values. (iii) $S(k)$ determined by fits of the models TP1, TP2, and TP3 is equal to $S(k)$ determined by numerical integration (Sec. III A), within the estimated uncertainty. (iv) Since models TP1 and TP2 are equally acceptable the discrepancy between the values of the parameters determined by both models will give an indication of their uncertainty. It appears that, going from TP1 to TP2, the parameters z_0, z_s, and ω_s only change 10—20%, whereas the parameters $\bar{z}_\Phi$, $\bar{z}_T$, and γ change up to a factor of 2. From the fits of model TP1 all parameters $\bar{z}_\Phi$, $\bar{z}_T$, γ, and ω_0 appeared to be highly correlated [positive correlations between the pairs $(\bar{z}_T,\gamma)$ and $(\bar{z}_\Phi,\omega_0)$, negative correlations between $(\bar{z}_\Phi,\bar{z}_T)$, $(\bar{z}_T,\omega_0)$, and (γ,ω_0)]. In the three-mode representation a strong positive correlation between (ω_0,z_s) and a strong negative correlation between (ω_0,ω_s) were observed. The parameters determined by the three-mode representation of model TP2 appeared to be only slightly, positively, correlated. In contrast, the correlations among the parameters in the generalized hydrodynamics representation of model TP2 were 3—4 times larger [negative correlations for $(\bar{z}_\Phi,\bar{z}_T)$ and $(\bar{z}_\Phi,\gamma)$ and positive for $(\bar{z}_T,\gamma)$]. For these reasons we consider the interpretation of $S(k,\omega)$, as determined from neutron scattering data, in terms of its eigenmodes more suitable than the interpretation in terms of generalized transport coefficients. (v) If $\gamma(k)$ is kept fixed at its hydrodynamic value (model TP3) the parameters $\bar{z}_\Phi$ and $\bar{z}_T$ [Fig. 13(b)] or $\Phi(k)$ and $D_T(k)$, (Fig. 14) agree reasonably well with the results from Refs. 8 and 29.

IV. CONCLUSIONS

We reported INS experiments on liquid neon at two densities at 35 K. After very careful corrections for all known experimental effects the reliability of the resulting $S(k,\omega)$ data was examined by means of three independent consistency checks. The agreement between the corrected $S(k,\omega)$ results from energy-gain and energy-loss data is satisfactory, the first frequency moment of $S(k,\omega)$ is equal to its theoretical value within the experimental uncertainty, and the static structure factor $S(k)$ obtained from numerical integration of $S(k,\omega)$ is in agreement with neutron diffraction results.

The first-order quantum effect in $\langle\omega^2\rangle$ (of order $\hbar^2$) can experimentally be observed in neon and is consistent with theoretical calculations. The magnitude of this effect is in neon a factor of nearly 10 larger than in argon at the corresponding thermodynamic state. The quasiclassical dynamic structure factor $\tilde{S}(k,\omega)$ of the present experiment has been compared with results of liquid argon at corresponding states. Except for some small differences the corresponding-state principle is shown to be valid. Discrepancies are present at k values around $k\sigma=2$ in the static structure factor $S(k)$, where $S(k)$ of argon is about 20% higher, and around $k\sigma=4$, where both the peak po-

sition ω_m of the longitudinal current correlation function $\tilde{C}_l(k,\omega)=\omega^2\tilde{S}(k,\omega)/k^2$ and the sound frequency ω_s are somewhat smaller in the case of neon. The origin of these deviations from CPS is unknown at present.

The present experimental data can very well be interpreted in terms of one (extended) heat mode and two (extended) sound modes. This three-mode description explains the dramatic change in shape of $S(k,\omega)$ going from small k values up to values around k_0, the first peak of $S(k)$. Near k_0 the sound modes become overdamped, resulting in a gap in the sound dispersion curve. The three poles z_{-1}, z_0, and z_{+1} of this description can be determined rather accurately. On the other hand, the k-dependent transport coefficients as used in Eq. (16), and associated with these three modes, are hard to determine unambiguously. It appeared that these coefficients, which are functions of z_{-1}, z_0, and z_{+1} [Eq. (A14)], are highly correlated when determined from $S(k,\omega)$ by least-squares fitting. In the past a few authors[8,29] have analyzed INS results by the generalized hydrodynamics description, Eq. (16), where $\gamma(k)$ is kept fixed at its hydrodynamic value. We showed that this restriction leads to unsatisfactory fits to the present $S(k,\omega)$ data for $k \lesssim 15$ nm^{-1}.

De Schepper *et al.*[34] demonstrated that demanding that the three-pole model obeys the sum rules up to the fourth [i.e., $R_n'(k)=R_n(k)$, $n=0,\ldots,4$] and, as a consequence, introduce relations between the eigenvalues z_{-1}, z_0, and z_{+1} does not yield a proper description of $S(k,\omega)$. This implies that if we want the model $S(k,\omega)$ to satisfy these sum rules additional Lorentzians of the sum in Eq. (10) are necessary or, alternatively, a z dependence of the generalized transport coefficients in Eq. (16) has to be introduced.

ACKNOWLEDGMENTS

Stimulating discussions with Dr. I. M. de Schepper are gratefully acknowledged. We thank Professor J. J. van Loef and Dr. P. Verkerk for their critical reading of the manuscript and A. J. W. Bouwman for his assistance during the course of the experiment.

APPENDIX: THE THREE-POLE APPROXIMATION OF $S(k,\omega)$

The Fourier and Laplace transforms of the intermediate scattering function $\hat{F}(k,t)$ are defined by

$$S(k,\omega)=\frac{1}{2\pi}\int_{-\infty}^{\infty} e^{-i\omega t}\hat{F}(k,t)dt \ , \tag{A1}$$

and

$$F(k,z)=\int_0^{\infty} e^{-zt}\hat{F}(k,t)dt \ , \tag{A2}$$

with

$$S(k,\omega)=\lim_{\epsilon\downarrow 0}\frac{1}{\pi}\mathrm{Re}F(k,z=i\omega+\epsilon) \ . \tag{A3}$$

The three-pole approximation of $F(k,z)$ is represented in three different ways.

Representation (a): the three-mode representation,

$$F(k,z)=S(k)\left[\frac{A_{-1}(k)}{z+z_{-1}(k)}+\frac{A_0(k)}{z+z_0(k)}+\frac{A_{+1}(k)}{z+z_{+1}(k)}\right] , \tag{A4}$$

$$\hat{F}(k,t)=S(k)\sum_{j=-1}^{+1}A_j(k)\exp[z_j(k)\,|\,t\,|\,] ,$$

where $A_0(k)$ and $z_0(k)$ are real and either $A_{\pm}(k)$ and $z_{\pm}(k)$ are real or complex conjugate pairs.

Representation (b): continued-fraction representation,

$$F(k,z)=S(k)\left[z+\Omega_0(k)+\cfrac{\Delta_1(k)}{z+\Omega_1(k)+\cfrac{\Delta_2(k)}{z+\Omega_2(k)}}\right]^{-1} , \tag{A5}$$

Representation (c): ratio of polynomials,

$$F(k,z)=S(k)\frac{z^2+A(k)z+B(k)}{z^3+C(k)z^2+D(k)z+E(k)} \ . \tag{A6}$$

The three representations are related to one another by (for the sake of clarity we will not explicitly display the k dependence)

$$\begin{aligned} A&=\Omega_1+\Omega_2 \ , \\ B&=\Omega_1\Omega_2+\Delta_2 \ , \\ C&=\Omega_0+\Omega_1+\Omega_2 \ , \\ D&=\Omega_0\Omega_1+\Omega_0\Omega_2+\Omega_1\Omega_2+\Delta_1+\Delta_2 \ , \\ E&=\Omega_0\Omega_1\Omega_2+\Omega_0\Delta_2+\Omega_2\Delta_1 \ , \end{aligned} \tag{A7}$$

and

$$\begin{aligned} A&=A_{-1}(z_0+z_{+1})+A_0(z_{-1}+z_{+1})+A_{+1}(z_{-1}+z_0) \ , \\ B&=A_{-1}z_0z_{+1}+A_0z_{-1}z_{+1}+A_{+1}z_{-1}z_0 \ , \\ C&=z_{-1}+z_0+z_{+1} \ , \\ D&=z_{-1}z_0+z_{-1}z_{+1}+z_0z_{+1} \ , \\ E&=z_{-1}z_0z_{+1} \ . \end{aligned} \tag{A8}$$

The short-time behavior, for $t>0$, of $\hat{F}(k,t)$ is described by the Taylor-series expansion

$$\hat{F}(k,t)=S(k)\sum_{n=0}^{\infty}\frac{t^n}{n!}R_n'(k) \ , \tag{A9}$$

with

$$R_n'(k)=\lim_{t\downarrow 0}\left[\frac{\partial^n}{\partial t^n}\frac{\hat{F}(k,t)}{S(k)}\right] ,$$

and the large-z behavior of $F(k,z)$, provided $\mathrm{Re}z>0$, by

$$F(k,z)=\frac{S(k)}{z}\sum_{n=0}^{\infty}R_n'(k)z^{-n} \ . \tag{A10}$$

We have chosen $R_0'(k)=1$ yielding $A_{-1}+A_0+A_{+1}=1$. The quantities $R_n'(k)$, expressed in the parameters appearing in the different representations, read as follows.

Representation (a):

$$R'_n=\sum_{j=-1}^{+1} A_j z_j^n \ . \tag{A11}$$

Representation (b):

$$\begin{aligned} R'_1&=-\Omega_0 \ , \\ R'_2&=\Omega_0^2-\Delta_1 \ , \\ R'_3&=-\Omega_0^3+2\Omega_0\Delta_1+\Omega_1\Delta_1 \ , \\ R'_4&=\Omega_0^4-3\Omega_0^2\Delta_1-2\Omega_0\Omega_1\Delta_1-\Omega_1^2\Delta_1+\Delta_1^2+\Delta_1\Delta_2 \ . \end{aligned} \tag{A12}$$

Representation (c):

$$\begin{aligned} R'_1&=A-C \ , \\ R'_2&=B-(CR'_1+D) \ , \\ R'_3&=-(CR'_2+DR'_1+E) \ , \\ R'_4&=-(CR'_3+DR'_2+ER'_1) \ . \end{aligned} \tag{A13}$$

Note that if in representation (b), Eq. (A5), both Ω_0 and Ω_1 are taken equal to zero, and if further $R'_2(k)=-\Delta_1=R_2(k)=-\omega_0^2$ and $R'_4(k)=\Delta_1^2+\Delta_1\Delta_2=R_4(k)=\omega_0^2\omega_l^2$ all sum rules up to the fourth are satisfied [Eq. (12)]. In this case the model is identical to the so-called viscoelastic model where $\tau(k)=\Omega_2^{-1}(k)$ is a wave-vector-dependent Maxwell relaxation time.[35]

Taking in representation (b) $S(k)=S(0)$, $\Omega_0=0$, $\Delta_1=\omega_0^2=\gamma^{-1}c_s k^2$, $\Omega_1=z_\Phi=\Phi k^2$, $\Omega_2=z_T=D_T k^2$, and $\Delta_2=(\gamma-1)\omega_0^2$ results in Eq. (15). From Eq. (A12) it follows that in the linearized hydrodynamic description $R'_3=\omega_0^2\Phi k^2$ is not equal to the correct sum rule $R_3=0$.

The generalized hydrodynamics representation discussed in Sec. III D [Eq. (16)] can be identified with the continued-fraction representation, Eq. (A5), with $\Omega_0=0$, $\omega_0^2=\Delta_1$, $\bar{z}_\Phi=\Omega_1\omega_0^{-1}$, $\bar{z}_T=\Omega_2\omega_0^{-1}$, and $\gamma-1=\Delta_2\omega_0^{-2}$. If we define $\bar{C}=C\omega_0^{-1}$, $\bar{D}=D\omega_0^{-2}$, $\bar{E}=E\omega_0^{-3}$, and $\bar{z}_j=z_j\omega_0^{-1}$ then the relation between the parameters acting in the generalized hydrodynamic representation and those in the three-mode representation is given by

$$\begin{aligned} \bar{z}_\Phi&=\bar{C}-\bar{E} \ , \\ \bar{z}_T&=\bar{E} \ , \\ \gamma&=\bar{D}-\bar{E}(\bar{C}-\bar{E}) \ , \end{aligned} \tag{A14}$$

with

$$\begin{aligned} \bar{C}&=\bar{z}_{-1}+\bar{z}_0+\bar{z}_{+1} \ , \\ \bar{D}&=\bar{z}_{-1}\bar{z}_0+\bar{z}_{-1}\bar{z}_{+1}+\bar{z}_0\bar{z}_{+1} \ , \\ \bar{E}&=\bar{z}_{-1}\bar{z}_0\bar{z}_{+1} \ . \end{aligned}$$

[1] P. Verkerk, *Neutron Inelastic Scattering 1977* (IAEA, Vienna, 1978), Vol. II, p. 53; Ph.D. thesis, University of Technology, Delft, 1985; P. Verkerk and A. A. van Well (unpublished); A. A. van Well and L. A. de Graaf, preceding paper, Phys. Rev. A **32**, 2384 (1985).

[2] A. A. van Well, P. Verkerk, L. A. de Graaf, J.-B. Suck, and J. R. D. Copley, Phys. Rev. A **31**, 3391 (1985).

[3] I. M. de Schepper, P. Verkerk, A. A. van Well, and L. A. de Graaf, Phys. Rev. Lett. **50**, 974 (1983).

[4] I. M. de Schepper, J. C. van Rijs, A. A. van Well, P. Verkerk, L. A. de Graaf, and C. Bruin, Phys. Rev. A **29**, 1602 (1984); C. Bruin *et al.* (unpublished).

[5] I. M. de Schepper and E. G. D. Cohen, Phys. Rev. A **22**, 287 (1980); J. Stat. Phys. **27**, 223 (1982).

[6] I. M. de Schepper, E. G. D. Cohen, and M. J. Zuilhof, Phys. Lett. **101A**, 399 (1984).

[7] M. J. Zuilhof, E. G. D. Cohen, and I. M. de Schepper, Phys. Lett. **103A**, 120 (1984).

[8] H. Bell, H. Moeller-Wenghoffer, A. Kollmar, R. Stockmeyer, T. Springer, and H. Stiller, Phys. Rev. A **11**, 316 (1975).

[9] J. Rouch, J. P. Boon, and P. A. Fleury, Physica A **88**, 347 (1977).

[10] L. A. de Graaf and B. Mozer, J. Chem. Phys. **55**, 4967 (1971).

[11] K. S. Singwi and A. S. Sjölander, Phys. Rev. **120**, 1093 (1960); R. Aamodt, K. M. Case, M. Rosenbaum, and P. F. Zweifel, *ibid.* **126**, 1165 (1962).

[12] V. F. Sears, Atomic Energy of Canada Limited (Chalk River, Ontario) Report No. AECL-8490, 1984 (unpublished).

[13] P. Verkerk, Nucl. Instrum. Methods **196**, 19 (1980).

[14] J. R. D. Copley, Comput. Phys. Commun. **7**, 289 (1974); **21**, 431 (1981); J. R. D. Copley *et al.* (unpublished).

[15] V. A. Rabinovitch, A. A. Wasserman, V. I. Nedostup, and L. S. Veksler, *Thermophysical Properties of Neon, Argon, Krypton and Xenon* (Standard, Moscow, 1976), in Russian.

[16] The fully corrected $S(k,\omega)$ is tabulated in Interuniversitair Reactor Instituut (Delft) Report No. IRI-132-84-13, 1984, available on request (unpublished).

[17] P. Verkerk and A. A. van Well, Nucl. Instrum. Methods Phys. Res. A **228**, 438 (1985).

[18] J. R. D. Copley, D. L. Price, and J. M. Rowe, Nucl. Instrum. Methods **107**, 501 (1973); **114**, 411 (1974).

[19] V. F. Sears, Phys. Rev. **185**, 200 (1969).

[20] L. Bewilogua, C. Gladun, and B. Kubsch, J. Low Temp. Phys. **4**, 299 (1971).

[21] K. Sköld, Phys. Rev. Lett. **19**, 1023 (1967).

[22] R. Evans and T. J. Sluckin, J. Phys. C **14**, 2569 (1981).

[23] B. M. Axilrod and E. Teller, J. Chem. Phys. **11**, 299 (1943).

[24] R. O. Watts and I. J. McGee, *Liquid State Chemical Physics* (Wiley, New York, 1976), p. 184.

[25] H. Fredrikze, Mol. Phys. **48**, 903 (1983).

[26] W. G. Madden and S. A. Rice, J. Chem. Phys. **72**, 4208 (1980).

[27] S. A. Mikhailenko, B. G. Dudar, and V. A. Schmidt, Fiz. Nizh. Temp. **1**, 224 (1975) [Sov. J. Low Temp. Phys. **1**, 109 (1975)].

[28] I. M. de Schepper, P. Verkerk, A. A. van Well, and L. A. de Graaf, Phys. Lett. **104A**, 29 (1984).

[29] P. A. Lonngi and L. S. Garcia-Colin, Can. J. Phys. **58**, 281 (1980).

[30] W. J. L. Buyers, V. F. Sears, P. A. Lonngi, and O. A. Lonngi, Phys. Rev. A **11**, 697 (1974).

[31] (a) R. D. Mountain, Adv. Mol. Relaxation Processes **9**, 225 (1976); (b) R. D. Mountain, in *Dynamics of Solids and Liquids by Neutron Scattering*, edited by S. W. Lovesey and T.

Springer (Springer, Berlin, 1977).
[32]H. Mori, Progr. Theor. Phys. **33**, 423 (1965).
[33]S. W. Lovesey, Phys. Rev. Lett. **53**, 401 (1984); I. M. de Schepper, P. Verkerk, A. A. van Well, L. A. de Graaf, and E. G. D. Cohen, Phys. Rev. Lett. **53**, 402 (1984).
[34]I. M. de Schepper, P. Verkerk, E. G. D. Cohen, A. A. van Well, and L. A. de Graaf, Phys. Rev. Lett. **54**, 158 (1985).
[35]S. W. Lovesey, Z. Phys. B **58**, 79 (1985).